JOURNAL OF THE ROYAL SOCIETY Interface

J. R. Soc. Interface (2011) **8**, 1019–1030
doi:10.1098/rsif.2010.0596
Published online 19 January 2011

Antibacterial burst-release from minimal Ag-containing plasma polymer coatings

Stefanie Lischer[1], Enrico Körner[1], Dawn J. Balazs[1], Dakang Shen[2,†], Peter Wick[1], Kathrin Grieder[1], Dieter Haas[2], Manfred Heuberger[1] and Dirk Hegemann[1,*]

[1]*Empa, Swiss Federal Laboratories for Materials Science and Technology, Lerchenfeldstrasse 5, CH-9014 St.Gallen, Switzerland*
[2]*Department of Fundamental Microbiology, University of Lausanne, CH-1015 Lausanne, Switzerland*

Biomaterials releasing silver (Ag) are of interest because of their ability to inhibit pathogenic bacteria including antibiotic-resistant strains. In order to investigate the potential of nanometre-thick Ag polymer (Ag/amino-hydrocarbon) nanocomposite plasma coatings, we studied a comprehensive range of factors such as the plasma deposition process and Ag cation release as well as the antibacterial and cytocompatible properties. The nanocomposite coatings released most bound Ag within the first day of immersion in water yielding an antibacterial burst. The release kinetics correlated with the inhibitory effects on the pathogens *Pseudomonas aeruginosa* or *Staphylococcus aureus* and on animal cells that were in contact with these coatings. We identified a unique range of Ag content that provided an effective antibacterial peak release, followed by cytocompatible conditions soon thereafter. The control of the *in situ* growth conditions for Ag nanoparticles in the polymer matrix offers the possibility to produce customized coatings that initially release sufficient quantities of Ag ions to produce a strong adjacent antibacterial effect, and at the same time exhibit a rapidly decaying Ag content to provide surface cytocompatibility within hours/days. This approach seems to be favourable with respect to implant surfaces and possible Ag-resistance/tolerance built-up.

Keywords: silver; plasma polymerization; antimicrobial; nanocomposite

1. INTRODUCTION

Silver (Ag) has been used for millenia in many applications including jewellery, tableware, currency or dental alloy [1]. The most important characteristic of Ag for hygienic and medical purposes is its disinfectant property owing to the release of silver cations (Ag^+). The first scientifically documented use of Ag as an antibacterial agent dates to 1881 when silver nitrate was used as an eye drop for prevention of gonococcal ophthalmia neonatorum [2,3]. With the emergence of antibiotics, the medical use of Ag declined. However, the interest in Ag is again increasing [4], as Ag ions are generally active against bacteria, including antibiotic-resistant strains. Especially, Ag nanoparticles are in use for medical applications such as Ag-impregnated catheters, wound dressings, prostheses coated or with embedded nanosilver [1,5] as well as for consumer products such as cosmetics or textiles [6]. Owing to their small size, Ag nanoparticles can exhibit different physico-chemical properties compared with those of the bulk metal. The higher surface area per mass results in a larger number of atoms that can interact with the environment [6–9]. It has been shown that metallic Ag poses a minimal health risk for the human body. Nevertheless, the direct interaction of Ag nanoparticles with the human body is a subject of ongoing investigations [10].

In our studies, Ag nanoparticles were grown *in situ* and bonded within a plasma polymer matrix-containing amino groups [11,12]. An important advantage of this type of low-pressure plasma coating is the high biocompatibility of the matrix polymer. With the choice of reactive gases (e.g. carbon dioxide (CO_2), nitrogen (N_2) or ammonia (NH_3)) and of monomer addition (e.g. hydrocarbons), the plasma technology allows formation of functionalized surfaces that are stable in aqueous environments [13–18]. Plasma technology is routinely used to prepare cell cultivation surfaces as substrates for cultivation of adherent cells. These products are treated by a low-pressure plasma process to create a hydrophilic finish on a polystyrene surface that enhances cell attachment and proliferation,

*Author for correspondence (dirk.hegemann@empa.ch).
†Present address: Department of Cellular and Molecular Medicine, University of Bristol, Bristol BS8 1TD, UK.

Received 28 October 2010
Accepted 8 December 2010

especially with the incorporation of nitrogen-containing cations [19].

When biomaterials are used as implants, they not only should promote cell growth, but ideally also exhibit initial antimicrobial properties [20]. This spurred us to investigate ultrathin plasma polymer coatings (25 nm thick) containing nanoparticles of Ag that could provide a burst-release of Ag ions to avoid bacterial colonization [21]. Although the overall amount of incorporated Ag is low, the Ag release can be adjusted to have a strong antibacterial effect within the first hours and to be consumed in this time frame. The initial Ag burst of the nanocomposites also helps in avoiding possible risks or potential of resistance and tolerance of bacterial cells to Ag [22,23], which might occur in a constantly low Ag-releasing environment. Recently, Landsdown reviewed the use of Ag in healthcare applications with focus on efficacy and safety aspects [24]. In the present study, we used the human pathogens *Pseudomonas aeruginosa* (Gram-negative) and *Staphylococcus aureus* (Gram-positive). These species are common nosocomial pathogens, which can cause implant-associated infections [20,25]. As model animal cells, we used the mouse fibroblast cell line 3T3 (according to the ISO norm 10993-5: biological evaluation of medical devices), which has the advantage of high reproducibility. Functional Ag/amino-hydrocarbon (Ag/a-C : H : N) metal–polymer nanocomposites were obtained by plasma polymerization in a gaseous mixture of ammonia and acetylene (NH_3/C_2H_2) combined with the co-sputtering of Ag atoms.

2. MATERIAL AND METHODS

2.1. Plasma polymerization and sputtering

In order to investigate the effects of both the functional plasma polymer and the Ag content in the Ag/a-C : H : N nanocomposites, a custom-built modular plasma reactor system was used to deposit Ag-containing or Ag-free amino-hydrocarbon (a-C : H : N) coatings. For co-sputtering of Ag, the Ag cathode was optionally introduced in the plasma chamber (asymmetric set-up), in contrast to Ag-free a-C : H : N plasma polymers that were produced in a symmetric reactor set-up [15]. The plasma exposure time was adjusted to deposit coatings of 25 nm thickness for all samples studied here. This coating thickness ensures that the substrates are uniformly coated, while possible film failure owing to internal or external stresses as known from thicker coatings is avoided [26]. For similar reasons, the deposition of an overlayer (or adlayer) was avoided.

2.2. Ag-free plasma polymer

Ag-free a-C : H : N coatings were deposited from gaseous mixtures of C_2H_4, NH_3 and argon (Ar) without Ag at the cathode. Therefore, a symmetric reactor set-up was chosen consisting of two plane parallel electrodes of the same size (30 cm in diameter) separated by a glass ring with a distance of 5 cm. The lower electrode, where the substrates were placed, was capacity-coupled to a 13.56 MHz radiofrequency (RF) excitation, while the upper electrode contained a gas shower for the homogeneous gas inlet controlled by flow meters. A roots pumping system evacuated the vacuum chamber through openings in the lower electrode to a base pressure of 5×10^{-2} Pa. Gas mixtures of variable NH_3/C_2H_4 ratios of 2 : 1 and 4 : 1 were used with varying power input ranging from 8 to 50 W at a fixed process pressure of 10 Pa in order to deposit nitrogen-functional plasma polymers.

2.3. Ag-containing plasma polymer

For the incorporation of Ag during the growing plasma polymer film, a Ag cathode (i.e. target, 16 cm in diameter) was mounted inside the plasma reactor close to the upper electrode, but insulated by a ceramic disc. In this asymmetric set-up, the Ag electrode was driven by 13.56 MHz RF excitation, while the lower electrode holding the substrates was grounded. This configuration results in a self-bias potential on the smaller Ag electrode, which leads to particle bombardment (sputtering) of the Ag target. Ag atoms are hence liberated into the plasma zone. Using proper experimental conditions, detrimental plasma polymer deposition on the Ag target can be prevented. Congruent processing parameters as those used for the Ag-free plasma polymers were employed to produce the metal–polymer nanocomposite coatings, i.e. NH_3/C_2H_4 flow ratio of 2 : 1 and 4 : 1, both with an admixture of Ar gas supporting the Ag sputtering, operated between 8 and 50 W at a pressure of 10 Pa. Beside comparable gas phase reactions, similar energetic conditions during the film growth were obtained for both symmetric and asymmetric reactor set-up yielding a comparable film functionality [27]. After plasma deposition, the chamber was re-evacuated for some time to remove any remaining by-products of the plasma deposition process. The substrates were subsequently removed and analysed by various surface characterization techniques as described below.

2.4. Continuous nano Ag coatings

Ag thin films were deposited on silicon (Si) wafers and tissue culture polystyrene (TCPS) Petri dishes as reference material using the asymmetric plasma configuration as described above. Ar-processing gas was used without further gases added, operated at a power of 50 W and a pressure of 10 Pa, in order to obtain a pure Ag sputtering. In the absence of polymerizing precursors, a continuous nanometre-thick metal layer (here: 25 nm) is formed. The Ag layer exhibited some surface roughness owing to the used process conditions (pressure of 10 Pa, 5 cm distance between Ag electrode and substrate), which was found to enhance the Ag ion release by about 30 per cent compared with a smooth sputter-deposited Ag layer (at a pressure of 1 Pa) [27].

2.5. X-ray photoelectron spectroscopy

In order to gain insight into the chemical nature of the Ag/a-C : H : N and a-C : H : N coatings, X-ray photoelectron spectroscopy (XPS) analyses were performed

on coated Si wafers (100) using a PHI 5600 LS X-ray photoelectron spectrometer (USA) equipped with a conventional hemispherical analyser. The X-ray source employed was a monochromatized Mg Kα (1235.6 eV) operated at 300 W. Spectral acquisition is performed under ultra-high vacuum (UHV; 10^{-10} Pa) conditions. Analysis was conducted using a take-off angle of 90° relative to the substrate surface. The pass energies were 58.7 and 187.8 eV for wide-scan and high-resolution elemental scans, respectively. These pass energies correspond to a step width of 0.80 and 0.025 eV, respectively. Charge compensation was performed with a self-compensating device using field-emitted low-energy electrons to keep the main carbon (C–H) component at a measured binding energy of 285.0 eV. The data reduction (atomic concentration, shift, curve fitting, etc.) was performed with CasaXPS v. 2.2.87 software. The sensitivity factors were 0.368, 0.314, 6.277, 0.498 and 0.733 for Si 2p, C 1s, Ag 3d, N 1s and O 1s, respectively. Spectra were fitted after a Shirley background subtraction.

2.6. Electron microscopy

The Ag nanocomposite coatings on Si substrates were thinned in cross-sectional view geometry with the tripod method. The final thickness suitable for electron transmission was achieved by an Ar^+ beam milling system (RES 101 from Baltec, UK). Low- and high-resolution transmission electron microscopies (HRTEM) were performed with a Jeol JEM FS2200 microscope (Japan).

2.7. Ag release kinetics analysed by inductively coupled plasma-optical emission spectrometry

A range of Ag/a-C : H : N coatings with varying Ag content were tested in a Ag release assay in comparison with continuous Ag thin films and Ag-free a-C:H:N polymer controls. Coatings were produced at high and low NH_3/C_2H_4 flow ratios, 2 : 1 and 4 : 1, respectively, operated between 8 and 50 W plasma input power. TCPS Petri dishes (Falcon) of 35 mm diameter were used as substrate material. The various coated dishes were exposed to 4 ml of deionized water (18 mΩ) at 37°C for a period of 1, 4, 6 and 14 days (long term) or for several hours (short term). These parameters correspond to important time and temperature settings of the biological testing described below. Following the liquid exposure, 1.5 ml samples of the supernatant were collected and submitted to the analysis techniques for the quantification of the Ag concentration. In order to identify the bulk Ag content of the coatings, as well as the Ag amount released from the coatings, inductively coupled plasma-optical emission spectrometry (ICP-OES) was performed on the various plasma-coated dishes using an Optima 3000, Perkin Elmer instrument, USA. Therefore, the Ag was dissolved in concentrated nitric acid and diluted with water. The Ag-containing solution was then introduced into the ICP-OES and optically analysed (Ag lines 328.068 and 338.289 nm). The calibration was performed using an external Ag standard solution of 1 mg ml^{-1}. A recovery rate was found between 98 and 101 per cent. The detection limit is lesser than or equal to 0.075 μg ml^{-1} in case of the dishes and lesser than or equal to 0.015 μg ml^{-1} (of Ag) concerning the solution. The concentration of released Ag (in ppm; parts per million) can then be converted into the release per area (in μg cm^{-2}) considering the volume of the solution (4 ml) and the sample size (9.6 cm^2), while the bulk Ag content can be given in mass per volume (in g cm^{-3}) regarding the adjusted film thickness (25 nm for all coatings). This enables a direct comparison with the density of Ag (10.49 g cm^{-3}) yielding an estimate for the volume fraction of incorporated Ag.

2.8. Antibacterial assays

Pseudomonas aeruginosa PAO1 (wild-type) and *S. aureus* 26AW (clinical isolate obtained from J. Entenza) were grown in Luria broth (LB (Difco); 10 g peptone, 5 g yeast extract, 10 g NaCl per litre) to exponential growth phase (about 10^9 colony forming units (CFU) per millilitre), centrifuged, washed with LB and diluted to 1.5×10^4 CFU ml^{-1} in LB agar containing 1 per cent KNO_3 and 1.5 per cent agar. One millilitre of this suspension was poured into 35 mm diameter TCPS Petri dishes (Falcon), which had been coated by Ag/a-C : H : N nanocomposites or Ag-free a-C : H : N. The thin layer of agar allowed close contact between the bacteria and the surface. The dishes were incubated at 37°C and the numbers of colonies were counted after 16–18 h. Three replicas were done for each sample and the experiment was repeated at least once to ensure reproducibility. The minimum inhibitory concentration (MIC) of Ag was determined for strain PAO1 in LB-containing $AgNO_3$ at a final concentration ranging from 1 to 100 μM. The inoculum was 10^5 CFU and incubation was overnight. The MIC was also determined on solid LB agar-containing $AgNO_3$ (final concentration of 1–100 μM). About 10^5 CFU were spread and the plates were incubated overnight. The MIC of $AgNO_3$ for *P. aeruginosa* was 12.5 μM. To determine bacterial growth on the surface not treated with Ag, bacterial suspensions were diluted 100-fold.

2.9. Cell culture conditions

Mouse fibroblast cell line 3T3 was obtained from the European Collection of Cell Culture (ECACC no. 85022108). Cells were grown in T25 flasks with the supplier's suggested medium Dulbecco's modified Eagle's medium (Gibco no. 41965) containing 2 mM glutamine, 10 per cent foetal calf serum and 1 per cent PSN (penicillin (5 mg ml^{-1}), streptomycin (5 mg ml^{-1}), neomycin (10 mg ml^{-1})) (Gibco) at 37° C with 5 per cent CO_2 over 8–10 passages. When the culture reached near confluence, the cells were trypsinized and seeded in plasma-coated 35 mm diameter TCPS Petri dishes (Falcon). All tested plasma coatings were pre-incubated in cell culture medium for 24 h to discard the first boost of Ag ions and to allow foetal calf serum proteins to adsorb to the coatings. The cell seeding density for

the MTT and DNA assay was 12 000 cells per 35 mm Petri dish and 6000 cells per Petri dish for the triple staining.

2.10. In vitro *cytotoxicity measurements*

The *in vitro* cytotoxicity assay is based on the ISO-Norm 10993-5: *biological evaluation of medical devices*. This assay evaluates if the test materials release toxic substances that have negative effects for cell culture. The cytotoxic effect on the cell activity and the cell proliferation is determined by the MTT and DNA measurements. MTT (3-(4,5-Dimethylthiazol-2-yl)-2,5-diphenyltetrazolium bromide) is reduced to a blue, water-insoluble MTT-formazane product by dehydrogenase activity in the mitochondria or cytoplasm of living cells. The amount of the formazane product is related to the quantity of cells and to their activity. The MTT assay was carried out after 4 and 6 days of exposition as described previously [28] with some modifications. Briefly, the culture dishes were once washed with pure culture medium (DMEM) and 250 µl per well of the MTT solution (5 mg ml^{-1}) (Sigma M2128) was added for 1 h at 37°C. Afterwards the supernatant was disposed and the blue MTT formazan product was dissolved in 1 ml solvent solution (90% ethanol, 10% HEPES-NaCl, pH 8.0) followed by gyratory shaking on a horizontal shaker for 15 min. The solvent solution of 100 µl was transferred to a 96-well plate and the absorbance of the supernatant was measured at 550 nm (Biotec Instruments ELx800, Witec AG, Littau, Switzerland). Wells without cells were used as blanks. The total DNA culture content was taken as an index for effects on cell proliferation. The DNA assay determines the amount of DNA in the cell culture. Fluorochrome bisbenzimidazol (Hoechst 33258) binds specifically to the DNA and its fluorescence can be detected at 460 nm. The intensity of the fluorescence is proportional to the amount of DNA and therefore proportional to the number of cells. The reaction is specific as fluorochrome bisbenzimidazol cannot bind to RNA or proteins. DNA was quantified on day 4 and day 6 using the Hoechst 33258 assay (Sigma 861405) as described previously [29] with some modifications. Briefly, the culture media of the Petri dishes was discarded and the cells were lysed by adding distilled water for 30 min. Afterwards, 100 µl of this solution were transferred to a 96-well plate, mixed with 100 µl of the Hoechst solution (20 µg ml^{-1} in TNE (10 mM Tris, 2 M NaCl and 1 mM EDTA) buffer) and incubated on a horizontal shaker for 1 h in the darkness. The fluorescence intensity was measured at 460 nm (Biotek Instruments FLx800, Witec AG, Littau, Switzerland). Before and at the end of the treatment period, all samples were analysed using a Nikon Diaphot light microscope (Nikon AG, Egg, Switzerland) combined with the digital imaging system Moticam 2300 (Mikroskop Technik Diethelm GmbH, Wagen, Switzerland). Each experiment was done independently three times. Per experiment all treatments were repeated two times per different type of plasma coating. Identically treated cultures were taken as replicate measure for statistical tests. Significant effects ($p < 0.05$) were determined using ANOVA two factorial Dunn–Bonferroni test (SPlus software).

2.11. *Triple staining actin, vinculin and nucleus*

On day 6, the cells were washed two times with phosphate-buffered saline (PBS) without glucose and treated with 4 per cent paraformaldehyde plus 0.2 per cent Triton-X for 8 min and washed again with PBS. The actin and vinculin staining were used to analyse the cell architecture. The actin filaments were stained with Alexa Fluor 488 phalloidin (1 : 40, Molecular Probes, A12 379) in PBS for 20 min. Vinculin, a focal adhesion protein, was stained by the first antibody h-Vin-1 monoclonal mouse IgG1 anti-vinculin (1 : 300, Sigma, V9131) in PBS solution with 1.5 per cent skim milk/PBS for 2 h and the second antibody Alexa Fluor 546-labelled goat anti-mouse IgG (1 : 400, Molecular Probes, A11030) in PBS solution with 1.5 per cent skim milk/PBS for 2 h. The nuclei of the cells were stained with the DNA marker BOBO-1 (Molecular Probes, B-3582) according to Kaiser *et al.* [30]. Triple-stained cells were imaged using the confocal laser scanning microscope LSM 510 (Carl Zeiss AG, Feldbach, Switzerland).

3. RESULTS

3.1. *Characterizing the plasma coatings*

The combination of polymerizable and etchable gases in a low-pressure RF plasma process leads to the deposition of a polymer-like layer with accessible functional groups [31,32]. Using gaseous mixtures of ethylene and ammonia, the plasma polymer consists of a cross-linked hydrocarbon matrix with nitrogen functionalities. These include amino groups that are stable against dissolution [13,32]. The degree of chemical functionality in the polymer matrix was tuned by changing the NH_3/C_2H_4 ratio, as monitored by XPS analysis (table 1). As expected, the nitrogen content was found to be increased at a higher NH_3/C_2H_4 ratio, which also resulted in lowered plasma polymer growth rates [31]. We also observe a higher wettability for higher N content [33]. The measured N/C ratio increased from approximately 0.4 for the process NH_3/C_2H_4 at 2 : 1 to a N/C ratio of approximately 0.6 for the process NH_3/C_2H_4 at 4 : 1. The nitrogen content of the a-C : H : N and Ag/a-C : H : N coatings was largely independent of the process power in the range of 8 to 50 W. Thus, an increase in power mainly resulted in an increase of the plasma polymer growth rate with higher deposition rates, as also previously reported [31,32]. Note that for the lower deposition rates as obtained for the NH_3/C_2H_4 ratio of 4 : 1, small differences in the ion bombardment might be responsible for the lowered N/C ratio within the symmetric set-up.

Working in the asymmetric reactor set-up and adding the sputtering gas Ar, the *in situ* incorporation of Ag nanoparticles into the growing functional plasma polymer matrix was achieved, again depending on the gas mixture and the power input. A TEM analysis of a Ag/a-C : H : N coating produced with a NH_3/C_2H_4

Table 1. Description and parameters of the 25 nm thick a-C : H : N plasma coatings used in this work. In the asymmetric plasma reactor set-up, a silver (Ag) electrode was mounted on one side. The Ag concentration was measured in the final coating by XPS (surface) and by ICP-OES (bulk).

reactor set-up	NH_3/C_2H_4	NH_3 (sccm)	C_2H_4 (sccm)	power input (W)	N/C	AgICP-OES (g cm^{-3})	AgXPS (at%)
sym	2 : 1	8	3.6	8	0.39	—	—
asym	2 : 1	8	3.6	8	0.39	0.19	0.70
asym	2 : 1	8	3.6	15	0.35	0.62	2.92
asym	2 : 1	8	3.6	25	0.36	1.21	4.27
asym	2 : 1	8	3.6	50	0.47	2.37	7.36
sym	4 : 1	8	2.1	8	0.42	—	—
asym	4 : 1	8	2.1	8	0.61	0.21	2.07
asym	4 : 1	8	2.1	15	0.60	0.87	4.22
asym	4 : 1	8	2.1	25	0.49	2.01	6.53
asym	4 : 1	8	2.1	50	0.56	4.16	10.67

ratio of 4 : 1 and a power input of 50 W was carried out to exemplify the growth of the Ag nanocomposites and the distribution of the Ag nanoparticles within the plasma polymer network (figure 1). A homogeneous Ag particle distribution was observed in the polymer matrix with an average particle diameter of 5–10 nm. The Ag nanoparticles were embedded in the plasma polymer, while the amount of Ag particles differed for varying power input [34]. Higher NH_3/C_2H_4 ratio as well as higher power input correlate with a higher Ag incorporation as evidenced by XPS surface analysis and ICP-OES measurements for the bulk composition (table 1). For better comparison, all coatings were deposited with the same thickness of 25 nm. The lowest Ag surface content of 0.7 at% was achieved in our series for a NH_3/C_2H_4 ratio of 2 : 1 and the lowest used power input of 8 W. The Ag content increased by a factor of 10 by increasing the power input to 50 W (keeping the ratio 2 : 1). The overall highest Ag surface concentration of 10.7 at% was obtained for the NH_3/C_2H_4 ratio of 4 : 1 at the power input of 50 W (figure 1). The bulk measurements show the same trends and also correlate with the Ag release measurements presented below. Besides the overall Ag content, the average particle size was also found to increase with power input [11]. Coatings obtained at a power input of 50 W showed a comparable Ag particle diameter for both NH_3/C_2H_4 ratios (2 : 1 and 4 : 1), while the particle number was found to be higher for higher gas ratios resulting in more Ag incorporation. A similar dependence of the Ag content and the particle diameter on the power input has also been observed for other Ag composite systems [34–38].

3.2. Ag release

Deionized water was used to quantify the kinetics of Ag^+ ion release from different Ag-containing nanocomposite plasma coatings. To avoid the possibility of precipitation of Ag^+ in water owing to oversaturation, the volume of water added to the plasma-coated Petri dishes was set to 4 ml in order to stay well below saturation at 20 ppm at 37°C (corresponding to 8.3 μg cm^{-2} for the used Petri dishes with an area of 9.6 cm^2). The maximum concentration of Ag released from the Ag/a-C : H : N coatings in cumulated measurements over 14 days was thus naturally limited to 5 ppm (2 μg cm^{-2}), while a plain metallic Ag surface (plasma sputtered) produced the highest concentration of 12 ppm (5 μg cm^{-2}) after two weeks of incubation in water. Figure 2 shows the Ag release from a plain metallic Ag coating deposited at 50 W and of the two experimental nanocomposite series using the NH_3/C_2H_4 ratios of 2 : 1 and 4 : 1 with varying power input. The Ag release has been converted to mass per area (μg cm^2). Both series (figure 2*a*,*b*) reveal a similar behaviour, showing a fast release (i.e. steep slope) within the first day, followed by a much slower release afterwards. Furthermore, a higher overall release occurred for Ag nanocomposites deposited with higher power input. As one would expect, more Ag ions were released from coatings with more Ag nanoparticles. During the release of Ag^+ ions, water presumably penetrates the plasma polymer matrix, facilitating surface oxidation of the embedded Ag nanoparticles owing to the oxygen dissolved in the water. Ag^+ ions are hydrated and can thus diffuse through the matrix according to equation (3.1):

$$4\,Ag_{(s)} + 4\,H_3O^+ + O_{2(aq)} \rightarrow 4\,Ag^+_{(aq)} + 6\,H_2O. \qquad (3.1)$$

The over-exponentially falling release rates (figure 3) can be explained by a diffusion-limited process in which the Ag nanoparticles nearest to the surface of the nanocomposite coating produce a fast initial release, i.e. short diffusion paths. The over-exponential first rise of Ag release is probably owing to Ag nanoparticle surfaces that are already in an oxidized state after plasma deposition [39], which largely facilitates Ag ion production. After about 1 day of immersion in water, the release rate was noticeably slower and asymptotically approached a constant low-residual release rate. Note that a considerable part (up to 60%) of the total incorporated Ag was released within those first 24 h. We recall the small coating thickness of 25 nm (table 1 and figure 2). Along the same lines, different release kinetics can be observed depending on the Ag size distribution and polymer matrix density. Figure 3 depicts the Ag release per day in deionized water for the coating series using 15 and 25 W power. The release rate of Ag ions clearly peaked during the first day

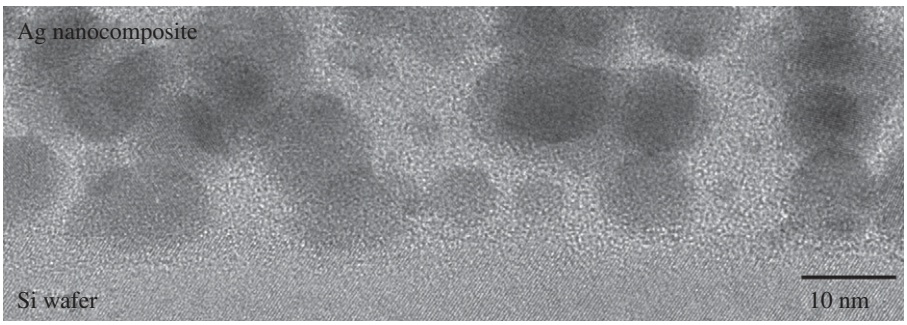

Figure 1. TEM cross-section of an Ag nanocomposite produced with a NH_3/C_2H_4 ratio of 4 : 1 and power input of 50 W.

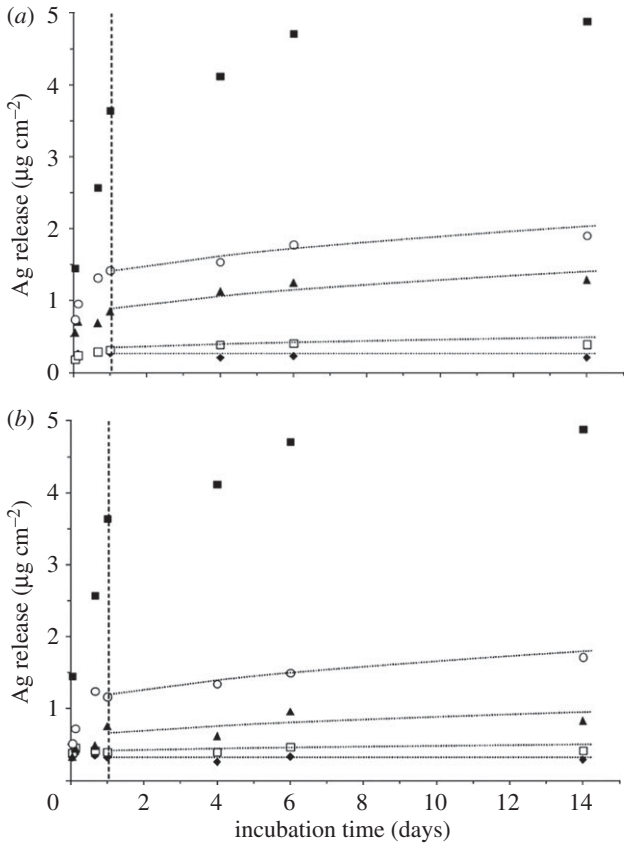

Figure 2. Total Ag release cumulated over time from the plasma coatings of series (*a*) $NH_3/C_2H_4 = 2:1$. (*b*) $NH_3/C_2H_4 = 4:1$. The amount of Ag in solution during the first day of incubation is indicated with the dashed line. For comparison, the total release from a plain metallic Ag layer (Ag ref.) is shown. Diamonds, 8 W; open squares, 15 W; triangles, 25 W; circles, 50 W; filled squares, Ag ref.

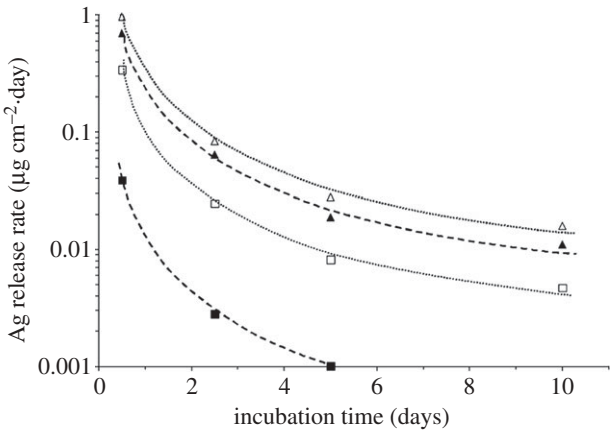

Figure 3. Total Ag released over time of incubation—comparing plasma coatings of type $NH_3/C_2H_4 = 2:1$ and 4 : 1 for 15 and 25 W power input. The silver (Ag) release rate of all nanocomposite coatings tested decays roughly an order of magnitude over the first 24 h. Filled squares, 4 : 1–15 W; open squares, 2 : 1–15 W; triangles, 4 : 1–25 W; open triangles, 2 : 1–25 W.

yielding an antibacterial burst. A different Ag release rate was obtained for the different NH_3/C_2H_4 gas ratios of 2 : 1 and 4 : 1. Although the 4 : 1 series produced coatings with higher overall Ag contents (table 1), the Ag release rate was smaller compared with the 2 : 1 series. We conclude that these differences are mainly owing to the influence of the plasma polymer matrix. While the coatings deposited with the NH_3/C_2H_4 gas ratio of 2 : 1 can be considered as polymer-like coatings (film density of 1.3–1.5 g cm^{-3}), the increased NH_3/C_2H_4 ratio yields more cross-linked and denser a-C : N : H coatings (1.6–1.8 g cm^{-3}) owing to a higher energy (ion bombardment) dissipated during film growth [13]. Therefore, water diffusion is generally facilitated in matrices produced at 2 : 1 gas ratios.

3.3. Antibacterial assay

The antibacterial assay was performed on the different Ag/a-C : H : N coatings as well as on Ag-free coatings as a control, with a NH_3/C_2H_4 flow ratio of 2 : 1 or 4 : 1 and power inputs ranging between 8 and 50 W. The coated Petri dishes were tested for their antibacterial properties either as deposited or after 1 day of pre-incubation in H_2O, which was afterwards discarded. A similar pre-incubation step was used in the cytotoxicity test described below to capture the situation after the initial Ag release peak. All Ag-free a-C : H : N coatings obtained with a NH_3/C_2H_4 ratio of 2 : 1 or 4 : 1 exhibited full bacterial contamination of the surface by *P. aeruginosa* and *S. aureus*, i.e. these coatings showed no antibacterial activity. The Ag/a-C : H : N nanocomposites, in contrast, revealed strongly reduced or absence of bacterial colonization depending on the power input. The nanocomposite coatings obtained at 8 W were more effective against *P. aeruginosa* than against *S. aureus*. The 2 : 1 and 4 : 1 gas

Table 2. Bacterial growth on Ag/a-C : H : N nanocomposites generated by a 4 : 1 or a 2 : 1 ratio of NH_3/C_2H_4 after inoculation with 1.5×10^4 CFU in 1 ml LB agar-containing KNO_3. The plasma coatings were tested (*a*) as deposited for their antibacterial properties or (*b*) after a 1 day exposure to 1 ml of H_2O to induce Ag^+ leaching. Bacterial growth is expressed as the percentage of colonies growing relative to those found in the uninhibited control.

coating parameter		bacterial growth (%)	
NH_3/C_2H_4	power (W)	*P. aeruginosa*	*S. aureus*
(*a*)			
4 : 1	8	0	7.5 ± 5
4 : 1	15	0	0
4 : 1	25	0	0
4 : 1	50	0	0
2 : 1	8	0	33 ± 10
2 : 1	15	0	0
2 : 1	25	0	0
2 : 1	50	0	0
(*b*)			
4 : 1	8	100	100
4 : 1	15	50 ± 1	100
4 : 1	25	20 ± 2	100
4 : 1	50	0	10 ± 1
2 : 1	8	100	100
2 : 1	15	50 ± 1	100
2 : 1	25	10 ± 1	100
2 : 1	50	0	0

ratios were effective against both pathogens for power inputs equal or greater than 15 W (table 2). In these experiments, bacteria were embedded in 1 ml of agar. Increasing the volume of the embedded bacterial suspension to 2 or 4 ml reduced the effective Ag^+ ion concentrations and no distinct antibacterial effect was observed for the power input of 8 W (data not shown). The samples pre-incubated with H_2O for 1 day showed a significant decrease of their antibacterial effectiveness (table 2). Only the coatings with the highest Ag content for both NH_3/C_2H_4 ratios of 2 : 1 and 4 : 1 exhibited an antibacterial activity against *S. aureus* and *P. aeruginosa*. The coatings with smaller amounts of Ag were not effective against *S. aureus* and less effective against *P. aeruginosa* (table 2). These findings demonstrate that the coatings provide a good short-term antimicrobial effect by releasing most of the incorporated Ag in the first 24 h. More long-term effects can be achieved at higher Ag incorporation. Thus, by adjusting the nanocomposite coatings, the antibacterial properties of the surface can be varied, depending on the application and the desired timescale of action.

3.4. Cytotoxicity assay

The cytotoxicity assay was performed with different Ag/a-C : H : N and Ag-free nanocomposite coatings using a NH_3/C_2H_4 flow ratio of 2 : 1 or 4 : 1 operated between 8 and 50 W. The nanocomposite coatings were produced 1 day before the cytotoxicity assay and pre-incubated with complete cell culture medium for 24 h. During this incubation time, a first boost of Ag^+ ions was released and foetal calf serum proteins adsorbed onto the coatings. Thereafter, the cell culture medium was discarded and the cells with fresh medium were seeded for the subsequent experiments. This incubation step allowed the analysis of the effect of the small and continuous Ag release to the 3T3 cells depending on the Ag amount in the coatings. This procedure was chosen to approximate conditions of an implant surface exposed to a moderate exchange with adjacent fluids within 1–2 days after implantation. Other than in the human body, the cells under *in vitro* conditions are directly seeded onto the coating surface and the cells interact immediately with the nanocomposites. Owing to the absence of a fluid flow in the polystyrene dish, the released Ag is accumulated and has a huge effect on the cells.

To evaluate the effects of the plasma coatings on 3T3 cell culture, cell density and morphology were observed by light and fluorescence microscopy. Figure 4 displays representative microscopic pictures of 3T3 cells on pre-incubated Ag-free, Ag/a-C : H : N nanocomposites using a NH_3/C_2H_4 ratio of 2 : 1 at 8, 15, 25 and 50 W power and on the polystyrene control on day 6. Figure 4 suggests that the a-C : H : N coating, *per se*, is a good cell-culture surface as similar cell densities were reproducibly recorded (figure 4*a*,*b*). The 3T3 cells also showed a high cell density on Ag/a-C : H : N nanocomposites operated by 8 W (figure 4*c*). With the increase of power input, a decrease in the cell density was observed (figure 4*d*,*e*) up to dead cells on coatings with 50 W (figure 4*f*). In addition to the light microscopy pictures, fluorescence images visualizing the cell architecture of 3T3 cells represented by the triple staining actin, vinculin and the nucleus were performed. For this staining only half of the cell number was seeded to analyse and monitor single cells. Figure 5 shows that cells nicely spread on the coatings determined by the actin (green) and vinculin, a member of the focal adhesion complex (red), indicating the strong cell adherence to the surface. This underlines that the Ag-free a-C : H : N matrix is intrinsically cytocompatible (figure 5*b*). It is also shown that the cells that attach on the Ag/a-C : H : N coatings operated at 8 and 15 W are nicely spread (figure 5*c*,*d*). Although only the 2 : 1 Ag/a-C : H : N coating was tested here, the same behaviour can be expected for higher power inputs and gas ratios owing to their comparable surface chemistries.

The quantitative analysis of cell functionality on the Ag/a-C : H : N and Ag-free nanocomposites was performed by the total DNA measurement and MTT assay on day 4 and 6. The values of the polystyrene control on day 4 were set to 100 per cent. The values on day 6 (related to the 100%) thereby show an increase in the cell population from day 4 to day 6. The total DNA content of the 3T3 cell culture was similar on the Ag-free a-C : H : N nanocomposites and the polystyrene control, here shown for the NH_3/C_2H_4 gas ratio of 4 : 1 and 2 : 1 at 8 W power (figure 6), as demonstrated by the statistical tests. The Ag/a-C : H : N nanocomposites permitted good cell proliferation on the plasma coatings that were operated with 8 W independently of the gas flow ratio. Ag/a-C : H : N nanocomposites that were produced at a power input

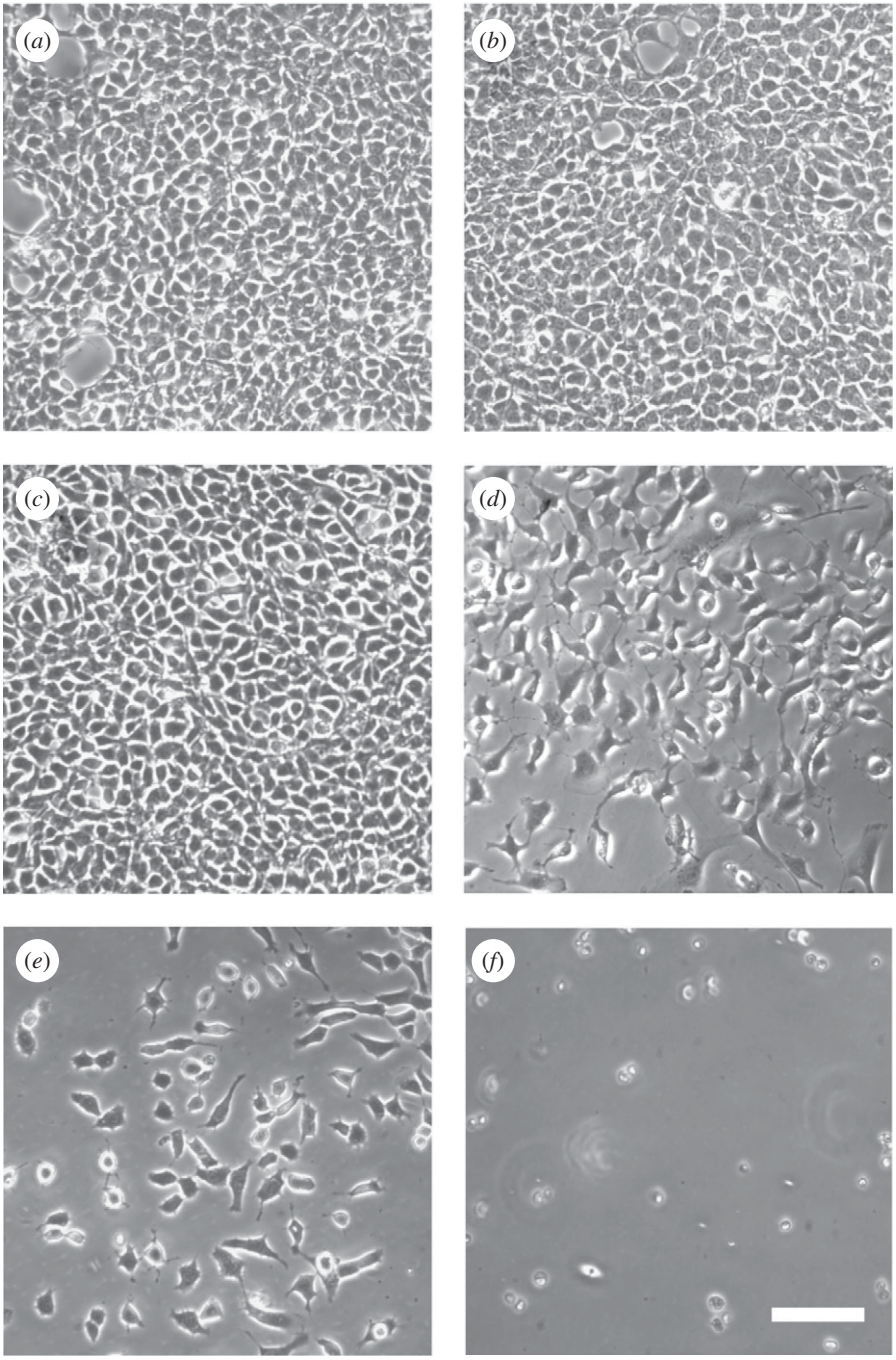

Figure 4. Representative light microscopy pictures of 3T3 cells on pre-incubated (*a*) a-C : H : N at 8 W, (*b*) polystyrene, (*c*) Ag/a-C : H : N at 8 W, (*d*) Ag/a-C : H : N at 15 W, (*e*) Ag/a-C : H : N at 25 W and (*f*) Ag/a-C : H : N at 50 W at day 6. The nanocomposites were deposited using a 2 : 1 ratio of NH_3/C_2H_4. Scale bar, 100 μm.

higher than 8 W had a decreased cell functionality, which indicates a negative effect of the released Ag for the cell functionality.

The MTT assay as an indicator of cell activity (figure 7) was performed in parallel and showed similar results. The pre-incubated Ag/a-C : H : N and Ag-free nanocomposites (NH_3/C_2H_4 ratio of 4 : 1 and 2 : 1) operated at a power input of 8 W promoted a high cell activity. The increase of the power input up to 50 W corresponding to an increased amount of Ag incorporation induced a decrease of the cell activity independently of the gas flow ratio. These results agree with the observation that the amount and particle size of Ag increases with power input, thereby increasing the overall Ag load in the nanocomposite coating [11].

The 3T3-tolerated Ag content for the pre-incubated Ag/a-C : H : N series with a NH_3/C_2H_4 ratio of 4 : 1 was in the range of 2.1–4.2 at%, while the corresponding range for the 2 : 1 series fell into 0.7–2.9 at% owing to the relatively higher Ag release from the latter coatings (figure 3).

4. DISCUSSION

This study reports the production of plasma nanocomposite coatings that allow controlled Ag release. The

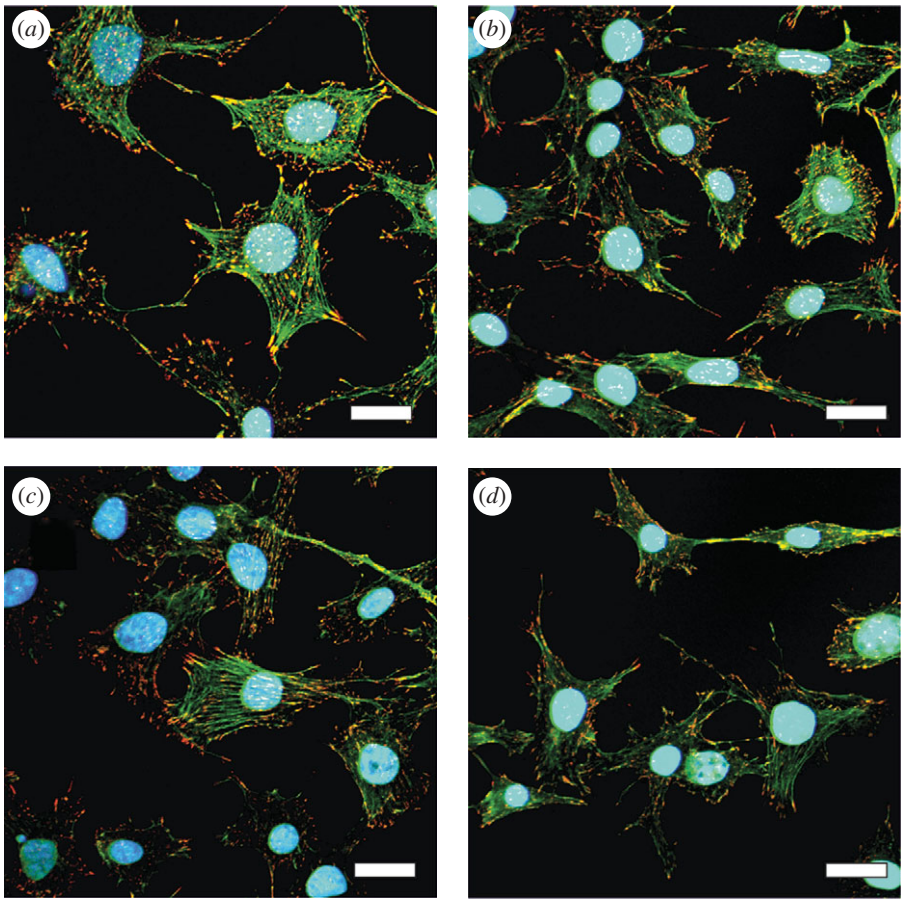

Figure 5. Representative microscopy pictures of 3T3 cells on day 6 on pre-incubated (*a*) polystyrene, (*b*) a-C : H : N at 8 W, (*c*) Ag/a-C : H : N at 8 W and (*d*) Ag/a-C : H : N at 15 W. The nanocomposites were prepared using a 2 : 1 ratio of NH_3/C_2H_4. Scale bar, 20 μm.

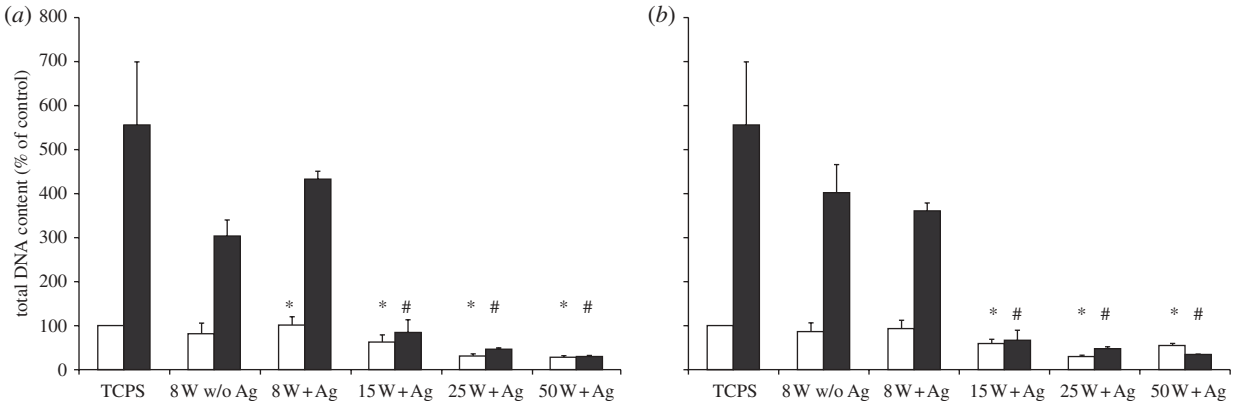

Figure 6. (*a*) DNA assay to determine the DNA content of 3T3 cells on pre-incubated Ag/a-C : H : N nanocomposites using a 4 : 1 ratio of NH_3/C_2H_4 at day 4 and 6. 3T3 cells were cultivated on tissue culture polystyrene (TCPS), on Ag-free a-C : H : N coatings (w/o Ag) and on Ag/a-C : H : N nanocomposites produced at 8, 15, 25 and 50 W. The data are expressed as mean ± s.e.m. of three independent experiments. (*b*) DNA assay to determine the DNA content of 3T3 cells on pre-incubated Ag/a-C : H : N nanocomposites using a 2 : 1 ratio of NH_3/C_2H_4 at day 4 and 6. 3T3 cells were cultivated on TCPS, on Ag-free a-C : H : N coatings (w/o Ag) and on Ag/a-C : H : N nanocomposites deposited at 8, 15, 25 and 50 W. The data are expressed as mean ± s.e.m. of three independent experiments. (*a*, *b*) Asterisk (*) indicates significantly different from control culture d4 $p < 0.05$, hash (#) indicates significantly different from control culture d6 $p < 0.05$. (*a*,*b*) Open bars, d4; filled bars, d6.

obtained antibacterial activity followed by cytocompatibility conditions after 1 day is a prerequisite for a comprehensive assessment of future medical applications. The plasma-coating technology is well established [17,38,40] and can be used to produce customized coatings on different support materials such as implants or catheters. Implants having antibacterial coatings could offer distinct advantages. For instance, despite numerous prophylactic measures, infections after total hip arthroplasties still occur in

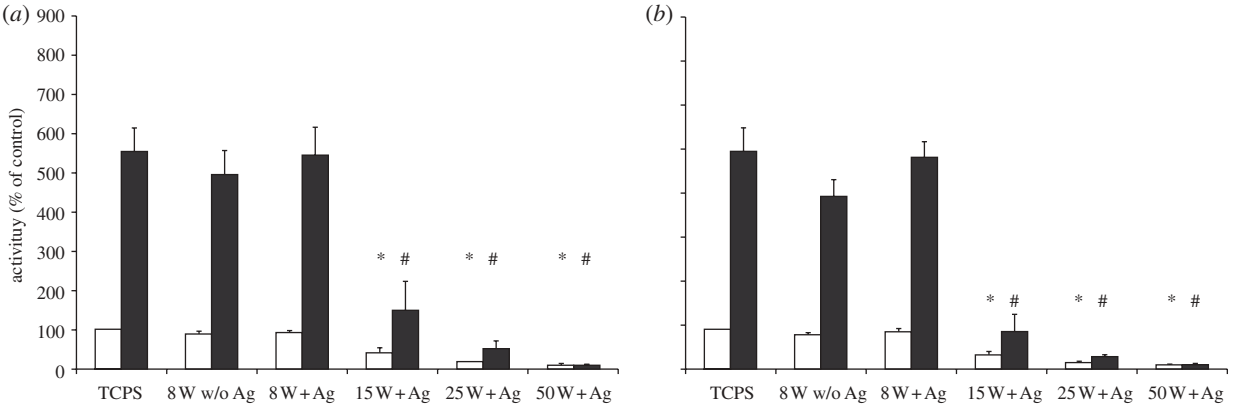

Figure 7. (*a*) MTT assay to determine the cell activity of 3T3 cells on pre-incubated Ag/a-C : H : N nanocomposites using a 4 : 1 ratio of NH_3/C_2H_4 at day 4 and 6. 3T3 cells were cultivated on TCPS, on Ag-free a-C : H : N coatings (w/o Ag) and on Ag/a-C : H : N nanocomposites prepared at 8, 15, 25 and 50 W. The data are expressed as mean ± s.e.m. of three independent experiments. (*b*) MTT assay to determine the cell activity of 3T3 cells on pre-incubated Ag/a-C : H : N nanocomposites using a 2 : 1 ratio of NH_3/C_2H_4 at day 4 and 6. 3T3 cells were cultivated on TCPS, on Ag-free a-C : H : N coatings (w/o Ag) and on Ag/a-C : H : N nanocomposites deposited at 8, 15, 25 and 50 W. The data are expressed as mean ± s.e.m. of three independent experiments. (*a*, *b*) Asterisk (*) indicates significantly different from control culture d4 $p < 0.05$, hash (#) indicates significantly different from control culture d6 $p < 0.05$. (*a*,*b*) Open bars, d4; filled bars, d6.

1–2% of the cases, and this rate may increase after revision surgery [41,42]. This means that between 1000 and 2500 patients annually undergo this type of complication in Germany alone [43]. Implant surfaces should not only enhance cell growth, but also show initial antimicrobial properties, to prevent bacterial infections that may occur after surgery and could lead to dramatic consequences for the patient resulting in unnecessary medical costs [20]. During the critical period following surgery, it is desirable to have an initial high release of antimicrobial agents [44]. The release of antimicrobial agents is especially more effective for rough surfaces or implants with niches than an ingested antibiotic treatment. The Ag-free polymer coating was not cytotoxic and residual Ag release observed after the initial peak release did not affect the cell functionality and spreading. These data are in agreement with recent studies, which have shown that primary amine groups on the plasma-treated surface promote cell attachment [17,45,46]. Our model study still does not address the fate or excretion of released Ag ions and therefore a more detailed assessment including *in vivo* tests will be necessary. The *in vivo* studies will provide more realistic conditions for the Ag/a-C : H : N coatings used, for example, for implants. In the body, the cells will not be directly in contact with the coated implants because it will take a while until the cells start to colonize the implant surface. However, it is important to have Ag release during this period in order to avoid bacterial infection.

The functionality of the a-C : H : N nanocomposites can mainly be influenced by the gas ratio of NH_3/C_2H_4 in the plasma reactor, while the nitrogen incorporation is independent of the power input in the range of 8–50 W [11,33]. With the asymmetric reactor set-up it is possible to incorporate Ag nanoparticles into the growing functional plasma polymer matrix. The power input as well as the gas ratio of NH_3/C_2H_4 determine the amount of Ag and the matrix properties of the nanocomposites and thereby controls the Ag release of the plasma coatings. The understanding and control of each process parameter of the nanocomposite coatings allow rapid development of surfaces with adjustable Ag release properties, which adds smart antibacterial functionality to current implant technology. The stability of such surface coatings on implants is paramount. NH_3/C_2H_4 plasma polymer coatings without Ag have been found to produce a permanent surface modification on textiles [33]. Denser and harder coatings, however, are prone to film failure (e.g. on implants) and tend to produce a lower Ag release [13,26,47]. In this study, the thickness of the functional plasma coatings was set to 25 nm to insure total coverage of the substrate surface in view of a reported interface of several nanometre [48]. Comparing the series with a NH_3/C_2H_4 ratio of 2 : 1 and 4 : 1, the former shows a higher Ag release. We think that this is due to better penetration of water into the less-dense plasma polymer matrix, where the Ag nanoparticles are embedded.

Ag release properties were assessed in water and the results are given in units of Ag mass per surface area. Therefore, a good comparison of the release properties between the different Ag nanocomposite samples is ensured; the same release unit also serves as a base for further application-oriented adjustments. *In vivo* released Ag^+ ions may react with constituents present in the environment (host cells and bacteria), resulting in binding of Ag^+. Our Ag release measurements, which were performed in water, can be regarded as a model system. It is worth mentioning that there was an excellent agreement between the Ag release kinetics and the biological assays. After pre-incubation, the Ag release from coatings deposited with a power input of 8 W was drastically reduced. Such coatings had antimicrobial activity limited to the first hours of incubation, immediately followed by excellent cytocompatibility. The Ag/a-C : H : N coatings deposited at 15 W, yielding Ag^+ ion concentrations of approximately 0.1 ppm after pre-incubation, still enabled cell attachment and spreading. In contrast higher power inputs, resulted in

sustained Ag^+ ion concentrations of approximately 1 ppm, which also suppressed cell activity. By adjusting the coating parameters, such as the NH_3/C_2H_4 ratio and the power input, we expect to be able to produce biomaterial surfaces that exhibit initial antibacterial properties as well as long-term biocompatibility. Thin uniform coatings are expected to be beneficial in view of possible film failure compared with thicker or harder coatings (or multi-layers) on implants. For this purpose, gradient Ag nanocomposite layers can also be regarded by changing the external plasma parameters during deposition. In conclusion, this work establishes the basic settings to produce such tailored functional plasma nanocomposite coatings that can be used to produce customized surfaces.

Part of the work was performed within the EU-funded project EMBEK1 'Development and analysis of polymer based multifunctional bactericidal materials', grant no. 211436 (7th framework programme). D.S. was supported by the VELUX Foundation. The work comprises four equally important parts: plasma coating (Balazs, Körner, Hegemann), Ag release kinetics (Körner, Grieder, Heuberger and Hegemann), antibacterial testing (Shen, Haas) and cytocompatible testing (Lischer, Wick); for this reason, several authors contributed equally.

REFERENCES

1 Chen, X. & Schluesener, H. J. 2008 Nanosilver: a nanoproduct in medical application. *Toxicol. Lett.* **176**, 1–12. (doi:10.1016/j.toxlet.2007.10.004)
2 Credé, C. 1881 Die Verhütung der Augenentzündung der Neugeborenen. *Archiv für Gynaekologie* **17**, 50–53. (doi:10.1007/BF01977793)
3 Russell, A. D. & Hugo, W. B. 1994 Antimicrobial activity and action of silver. *Prog. Med. Chem.* **31**, 351–370. (doi:10.1016/S0079-6468(08)70024-9)
4 Arora, S., Jain, J., Rajwade, J. M. & Paknikar, K. M. 2008 Cellular responses induced by silver nanoparticles: *in vitro* studies. *Toxicol. Lett.* **179**, 93–100. (doi:10.1016/j.toxlet.2008.04.009)
5 Asharani, P. V., Low Kah Mun, G., Hande, M. P. & Valiyaveettil, S. 2009 Cytotoxicity and genotoxicity of silver nanoparticles in human cells. *ACS Nano.* **3**, 279–290. (doi:10.1021/nn800596w)
6 Wijnhoven, S. W. P. *et al.* 2009 Nano-silver—a review of available data and knowledge gaps in human and environmental risk assessment. *Nanotoxicology* **3**, 109–138. (doi:10.1080/17435390902725914)
7 Hwang, E. T., Lee, J. H., Chae, Y. J., Kim, Y. S., Kim, B. C., Sang, B. I. & Gu, M. B. 2008 Analysis of the toxic mode of action of silver nanoparticles using stress-specific bioluminescent bacteria. *Small* **4**, 746–750. (doi:10.1002/smll.200700954)
8 Lok, C. N., Ho, C. M., Chen, R., He, Q. Y., Yu, W. Y., Sun, H., Tam, P. K., Chiu, J. F. & Che, C. M. 2007 Silver nanoparticles: partial oxidation and antibacterial activities. *J. Biol. Inorg. Chem.* **12**, 527–534. (doi:10.1007/s00775-007-0208-z)
9 Pal, S., Tak, Y. K. & Song, J. M. 2007 Does the antibacterial activity of silver nanoparticles depend on the shape of the nanoparticle? A study of the Gram-negative bacterium *Escherichia coli*. *Appl. Environ. Microbiol.* **73**, 1712–1720. (doi:10.1128/AEM.02218-06)
10 Drake, P. L. & Hazelwood, K. J. 2005 Exposure-related health effects of silver and silver compounds: a review. *Ann. Occup. Hyg.* **49**, 575–585. (doi:10.1093/annhyg/mei019)
11 Balazs, D., Hossain, M., Brombacher, E., Fortunato, G., Körner, E. & Hegemann, D. 2007 Multi-functional nano composite plasma coatings—enabling new applications in biomaterials. *Plasma Process. Polym.* **4**, 380–385. (doi:10.1002/ppap.200731004)
12 Hegemann, D., Hossain, M. & Balazs, D. 2007 Nanostructured plasma coatings to obtain multifunctional textile surfaces. *Progr. Org. Coat.* **58**, 237–240. (doi:10.1016/j.porgcoat.2006.08.027)
13 Guimond, S., Hanselmann, B., Amberg, M. & Hegemann, D. 2010 Plasma functionalization of textiles: specifics and possibilities. *Pure Appl. Chem.* **82**, 1239–1245. (doi:10.1351/PAC-CON-09-10-38)
14 Hegemann, D., Körner, E. & Guimond, S. 2009 Plasma polymerization of acrylic acid revisited. *Plasma Process. Polym.* **6**, 246–254. (doi:10.1002/ppap.200800089)
15 Körner, E., Fortunato, G. & Hegemann, D. 2009 Influence of RF plasma reactor setup on carboxylated hydrocarbon coatings. *Plasma Process. Polym.* **6**, 119–125. (doi:10.1002/ppap.200800102)
16 Mwale, F., Wang, H. T., Nelea, V., Luo, L., Antoniou, J. & Wertheimer, M. R. 2006 The effect of glow discharge plasma surface modification of polymers on the osteogenic differentiation of committed human mesenchymal stem cells. *Biomaterials* **27**, 2258–2264. (doi:10.1016/j.biomaterials.2005.11.006)
17 Siow, K., Britcher, L., Kumar, S. & Griesser, H. 2006 Plasma methods for the generation of chemically reactive surfaces for biomolecule immobilization and cell colonization—a review. *Plasma Process. Polym.* **3**, 392–418. (doi:10.1002/ppap.200600021)
18 Truica-Marasescu, F. & Wertheimer, M. 2008 Nitrogen-rich plasma-polymer films for biomedical applications. *Plasma Process. Polym.* **5**, 44–57. (doi:10.1002/ppap.200700077)
19 Chilkoti, A., Schmierer, A. E., Pérez-Luna, V. H. & Ratner, B. D. 1995 Investigating the relationship between surface chemistry and endothelial cell growth: partial least-squares regression of the static secondary ion mass spectra of oxygen-containing plasma-deposited film. *Anal. Chem.* **67**, 2883–2891. (doi:10.1021/ac00113a024)
20 Hetrick, E. M. & Schoenfisch, M. H. 2006 Reducing implant-related infections: active release strategies. *Chem. Soc. Rev.* **35**, 780–789. (doi:10.1039/b515219b)
21 Poelstra, K. A., Barekzi, N. A., Rediske, A. M., Felts, A. G., Slunt, J. B. & Grainger, D. W. 2002 Prophylactic treatment of Gram-positive and Gram-negative abdominal implant infections using locally delivered polyclonal antibodies. *J. Biomed. Mater. Res.* **60**, 206–215. (doi:10.1002/jbm.10069)
22 Chopra, I. 2007 The increasing use of silver-based products as antimicrobial agents: a useful development or a cause for concern? *J. Antimicrob. Chemother.* **59**, 587–590. (doi:10.1093/jac/dkm006)
23 Wright, J. B., Lam, K. & Burrell, R. E. 1998 Wound management in an era of increasing bacterial antibiotic resistance: a role for topical silver treatment. *Am. J. Infect. Control* **26**, 572–577. (doi:10.1053/ic.1998.v26.a93527)
24 Lansdown, A. B. G. 2010 *Silver in healthcare: its antimicrobial efficacy and safety in use*. Issues in toxicology No. 6, Cambridge, UK: Royal Society of Chemistry, 2010.
25 Sadikot, R. T., Blackwell, T. S., Christman, J. W. & Prince, A. S. 2005 Pathogen–host interactions in *Pseudomonas aeruginosa* pneumonia. *Am. J. Respir. Crit. Care Med.* **171**, 1209–1223. (doi:10.1164/rccm.200408-1044SO)

26 Hauert, R. 2003 A review of modified DLC coatings for biological applications. *Diam. Relat. Mater.* **12**, 583–589. (doi:10.1016/S0925-9635(03)00081-5)

27 Hegemann, D., Amberg, M., Hanselmann, B., Guimond, S. & Körner, E. 2010. Nanostructured plasma coatings for medical applications. In *Proc. ESF Workshop 'Manipulation of Biomaterials Surfaces by Plasma Processing'.* Romania: Iasi.

28 Mosmann, T. 1983 Rapid colorimetric assay for cellular growth and survival: application to proliferation and cytotoxicity assays. *J. Immunol. Methods* **65**, 55–63. (doi:10.1016/0022-1759(83)90303-4)

29 Daxhelet, G. A., Coene, M. M., Hoet, P. P. & Cocito, C. G. 1989 Spectrofluorometry of dyes with DNAs of different base composition and conformation. *Anal. Biochem.* **179**, 401–403. (doi:10.1016/0003-2697(89)90152-8)

30 Kaiser, J. P., Wick, P., Manser, P., Spohn, P. & Bruinink, A. 2008 Single walled carbon nanotubes (SWCNT) affect cell physiology and cell architecture. *J. Mater. Sci. Mater. Med.* **19**, 1523–1527. (doi:10.1007/s10856-007-3296-y)

31 Hegemann, D. & Hossain, M. 2005 Influence of non-polymerizable gases added during plasma polymerization. *Plasma Process. Polym.* **2**, 554–562. (doi:10.1002/ppap.200500041)

32 Hossain, M., Herrmann, A. & Hegemann, D. 2007 Incorporation of accessible functionalities in nanoscaled coatings on textiles characterized by coloration. *Plasma Process. Polym.* **4**, 135–144. (doi:10.1002/ppap.200600085)

33 Hossain, M., Hegemann, D., Fortunato, G., Herrmann, A. & Heuberger, M. 2007 Plasma deposition of permanent superhydrophilic a-C : H : N films on textiles. *Plasma Process. Polym.* **4**, 471–481. (doi:10.1002/ppap.200600214)

34 Körner, E., Aguirre, M. H., Ritter, A., Michel, E., Fortunato, G., Rühe, J. & Hegemann, D. 2010 Formation and distribution of silver nanoparticles in a functional plasma polymer matrix and the related Ag^+ release properties. *Plasma Process. Polym.* **7**, 619–625. (doi:10.1002/ppap.200900163)

35 Biederman, H., Martinu, L., Slavinska, D. & Chudacek, I. 1988 Plasma deposition and properties of composite metal/polymer and metal/hard carbon films. *Pure Appl. Chem.* **60**, 607–618. (doi:10.1351/pac198860050607)

36 Kay, E. 1986 Synthesis and properties of metal clusters in polymeric matrices. *Z. Phys. D At. Mol. Clusters* **3**, 251–262. (doi:10.1007/BF01384814)

37 Perrin, J., Despax, B., Hanchett, V. & Kay, E. 1986 Microstructure and electrical conductivity of plasma deposited gold/fluorocarbon composite films. *J. Vac. Sci. Technol. A* **4**, 46–51. (doi:10.1116/1.573496)

38 Sardella, E., Favia, P., Gristina, R., Nardulli, M. & D'agostino, R. 2006 Plasma-aided micro- and nanopatterning processes for biomedical applications. *Plasma Process. Polym.* **3**, 456–469. (doi:10.1002/ppap.200600041)

39 Hlídek, P., Biederman, H., Choukourov, A. & SlavínskÁ, D. 2009 Behavior of polymeric matrices containing silver inclusions, 2-oxidative aging of nanocomposite Ag/C:H and Ag/C:H:O films. *Plasma Process. Polym.* **6**, 34–44. (doi:10.1002/ppap.200800084)

40 Förch, R., Zhang, Z. & Knoll, W. 2005 Soft plasma treated surfaces: tailoring of structure and properties for biomaterial applications. *Plasma Process. Polym.* **2**, 351–372. (doi:10.1002/ppap.200400083)

41 Anagnostakos, K., Schmid, N. V., Kelm, J., Grun, U. & Jung, J. 2009 Classification of hip joint infections. *Int. J. Med. Sci.* **6**, 227–233.

42 Fink, B. 2009 Revision of late periprosthetic infections of total hip endoprostheses: pros and cons of different concepts. *Int. J. Med. Sci.* **6**, 287–295.

43 Haaker, R., Senge, A., Kramer, J. & Rubenthaler, F. 2004 Osteomyelitis after endoprostheses. *Orthopade* **33**, 431–438. (doi:10.1007/s00132-003-0624-x)

44 Anderson, J. H. 2001 Biological responses to materials. *Annu. Rev. Mater. Res.* **31**, 81. (doi:10.1146/annurev.matsci.31.1.81)

45 Finke, B., Luethen, F., Schroeder, K., Mueller, P. D., Bergemann, C., Frant, M., Ohl, A. & Nebe, B. J. 2007 The effect of positively charged plasma polymerization on initial osteoblastic focal adhesion on titanium surfaces. *Biomaterials* **28**, 4521–4534. (doi:10.1016/j.biomaterials.2007.06.028)

46 Zhang, W., Luo, Y., Wang, H., Pu, S. & Chu, P. K. 2009 Biocompatibility of silver and copper plasma doped polyethylene. *Surf. Coat. Technol.* **203**, 2550–2553. (doi:10.1016/j.surfcoat.2009.02.073)

47 Bertaux, E., Le marec, E., Crespy, D., Rossi, R. & Hegemann, D. 2009 Effects of siloxane plasma coating on the frictional properties of polyester and polyamide fabrics. *Surf. Coat. Technol.* **204**, 165–171. (doi:10.1016/j.surfcoat.2009.07.016)

48 Hegemann, D., Schütz, U. & Oehr, C. 2005 RF plasma deposition of SiO_x and a-C:H as barrier coatings on polymers. In *Plasma processes and polymers* (eds R. D'Agostino, P. Favia, C. Oehr & M. R. Wertheimer), pp. 23–37. Weinheim, Germany: Wiley-VCH.